ACS APPLIED MATERIALS & INTERFACES

Research Article

www.acsami.org

Highly Sensitive, Flexible, and Wearable Pressure Sensor Based on a Giant Piezocapacitive Effect of Three-Dimensional Microporous Elastomeric Dielectric Layer

Donguk Kwon,[†] Tae-Ik Lee,[†] Jongmin Shim,[‡] Seunghwa Ryu,[†] Min Seong Kim,[†] Seunghwan Kim,[†] Taek-Soo Kim,[†] and Inkyu Park*[,†,§]

[†]Department of Mechanical Engineering, Korea Advanced Institute of Science and Technology (KAIST), 291 Daehak-ro, Yuseong-gu, Daejeon 305-701, South Korea

[‡]Department of Civil, Structural and Environmental Engineering, University at Buffalo, Buffalo, New York 14260, United States

[§]KAIST Institute (KI) for the NanoCentury, Korea Advanced Institute of Science and Technology (KAIST), 291 Daehak-ro, Yuseong-gu, Daejeon 305-701, South Korea

Supporting Information

ABSTRACT: We report a flexible and wearable pressure sensor based on the giant piezocapacitive effect of a three-dimensional (3-D) microporous dielectric elastomer, which is capable of highly sensitive and stable pressure sensing over a large tactile pressure range. Due to the presence of micropores within the elastomeric dielectric layer, our piezocapacitive pressure sensor is highly deformable by even very small amounts of pressure, leading to a dramatic increase in its sensitivity. Moreover, the gradual closure of micropores under compression increases the effective dielectric constant, thereby further enhancing the sensitivity of the sensor. The 3-D microporous dielectric layer with serially stacked springs of elastomer bridges can cover a much wider pressure range than those of previously reported micro-/nanostructured sensing materials. We also investigate the applicability of our sensor to wearable pressure-sensing devices as an electronic pressure-sensing skin in robotic fingers as well as a bandage-type pressure-sensing device for pulse monitoring at the human wrist. Finally, we demonstrate a pressure sensor array pad for the recognition of spatially distributed pressure information on a plane. Our sensor, with its excellent pressure-sensing performance, marks the realization of a true tactile pressure sensor presenting highly sensitive responses to the entire tactile pressure range, from ultralow-force detection to high weights generated by human activity.

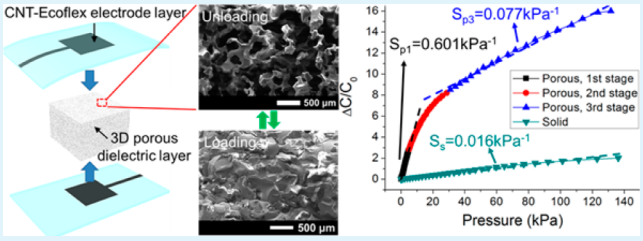

KEYWORDS: *microporous elastomers, piezocapacitive effects, flexible sensors, wearable sensors, pressure sensors*

INTRODUCTION

Flexible pressure sensors have been attracting much attention due to their importance in relation to various advanced applications, such as electronic skin,[1−4] electronic textiles,[5−7] flexible touch displays,[8,9] soft robotics,[10−13] mobile healthcare aids,[14,15] and energy harvesting.[16−18] In general, these tasks involve human tactile pressure interactions between the user and the device from mild touches (0−10 kPa, low-pressure regime) to object handling levels (10−100 kPa, medium-pressure regime).[15,19] Considering practical uses in these applications, high sensitivity in a low-pressure regime is essential for delicate pressure sensing which surpasses the sensing capability of human skin. Moreover, it is necessary to maintain reasonably high sensitivity over a wide dynamic range up to 100 kPa, which can cover the overall tactile pressure range.

Previously, many studies reported successful pressure-sensing demonstrations with various working principles, such as piezoresistivity,[20−23] capacitance,[8,24−27] and piezoelectricity,[28−30] etc.[18,31,32] In particular, recent efforts have focused on improving the sensitivity of sensors in low-pressure regimes.[15] Specifically, a number of microstructured materials have been suggested in an effort to enhance sensitivity in the low-pressure regime by modifying the bulk mechanical and electrical properties of materials. For piezocapacitive sensors, a microstructured polymer dielectric material was incorporated within a parallel-plate capacitor to realize a larger capacitance change than that of an unstructured dielectric material at an identical pressure level.[14,19,33−35] Commercially available polymer foams were employed as a dielectric layer in a piezocapacitive pressure sensor to improve the sensing capability via the modulated elastic property of the dielectric layer.[33] Its poor sensitivity, however, made it unsuitable for the detection of low pressure levels, such as tactile sensing, as the

Received: April 9, 2016
Accepted: June 10, 2016
Published: June 10, 2016

DOI: 10.1021/acsami.6b04225
ACS Appl. Mater. Interfaces 2016, 8, 16922−16931

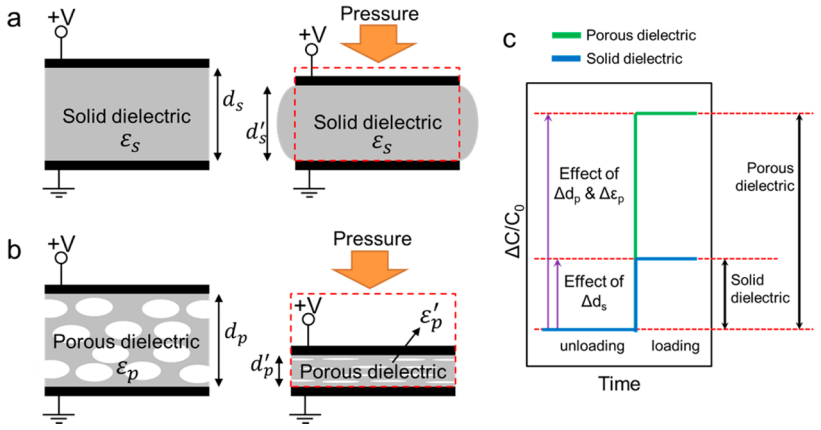

Figure 1. Comparison of pressure-sensing mechanisms between sensors using a solid elastomeric dielectric layer and a porous elastomeric dielectric layer. (a) Schematic illustration of a capacitive pressure sensor using a solid elastomeric dielectric layer and its geometrical change upon barreling after being compressed in response to external pressure. (b) Schematic illustration of a piezocapacitive pressure sensor using a porous elastomeric dielectric layer and the geometrical change without barreling due to the closure of pores in response to the same external pressure. (c) Relative changes of the capacitances of pressure sensors using solid and porous elastomeric dielectric layers induced by identical levels of external loading. The synergy of the larger deformation by the reduced stiffness and the increased effective dielectric constant by the closure of the air gap dramatically amplifies the capacitance change.

resolution was only ~1 kPa. A two-dimensional (2-D) pyramid-shaped microstructure array as a dielectric layer of a piezocapacitive pressure sensor was also reported, offering great sensitivity as well as short response and recovery times.[14,19,34,35] However, this device requires a microstructured silicon mold that should be fabricated with expensive microfabrication processes. In addition, the performance of the sensor is only valid within a relatively narrow pressure range, not enough to cover the entire tactile pressure range up to 100 kPa. On the other hand, piezoresistive pressure sensors based on conductive microstructured materials were reported to provide enhanced elasticity and dramatic changes of the resistance to sensing materials.[36−43] The sensing materials of these piezoresistive pressure sensors were prepared by (i) coating conductive materials (e.g., metal, graphene, single-walled nanotubes, and conductive polymers) onto micro-structured templates and (ii) directly forming conductive microstructures with a conductive material−elastomer mixture.[36−42] However, they did not cover the entire tactile pressure range, commonly featuring only limited dynamic ranges. Moreover, they showed a sharp decrease of sensitivity in a high-pressure range, which is unacceptable for practical use in relation to human tactile pressure interactions. To overcome these limitations, a piezoresistive sensor based on the foam-like structure of laser-scribed graphene was demonstrated with a wide pressure-sensing range.[43] Despite the wide working range, however, this sensor showed highly nonlinear and unstable responses at low pressures of less than 50 kPa due to the unstable changes of the contact area between graphene microstructures.

Herein, we report a flexible and wearable piezocapacitive pressure sensor based on a three-dimensional (3-D) micro-porous dielectric elastomer,[44] which is capable of highly sensitive and stable pressure sensing over the entire tactile pressure range (~130 kPa) via a facile and cost-effective process. The microporous dielectric elastomer can provide perfectly reversible and elastic compressive behavior while micropores are closed and opened without viscoelastic behavior, which is generally considered as the major cause of hysteresis. Based on the compressive behavior of the micro-porous structure under external pressure, we successfully achieved outstanding sensor performance with high sensitivity of 0.601 kPa^{-1} at 5 kPa and a wide dynamic range of 0.1 Pa to 130 kPa without a significant reduction in the sensitivity. In addition, it was demonstrated that the sensor could easily be integrated into robotic fingers for the monitoring of the grasping force during seizing motions and into the human body to monitor the pulse at the wrist. Finally, we demonstrated the performance of a sensor array pad which recognizes spatially distributed pressure information on a plane.

EXPERIMENTAL SECTION

Preparation of Porous Ecoflex for Dielectric Layer. A porous Ecoflex dielectric layer was formed by molding the Ecoflex elastomer within a sugar cube template. The Ecoflex (Ecoflex Shore hardness, 00−30; Smooth-On, Inc., Macungie, PA, USA) prepolymer solution was prepared by mixing a base and a curing agent at a weight ratio of 1:1, after which a sugar cube was immediately immersed in the Ecoflex prepolymer solution. The Ecoflex prepolymer solution with the sugar cube was degassed within a vacuum chamber and cured in a convection oven at 60 °C for 1 h. The sugar portion of the cured Ecoflex-sugar cube was dissolved by water and consequently dried in air.

Preparation of Carbon Nanotube−Ecoflex Nanocomposite Film for Electrode Layer. Carbon nanotube (CNT)−Ecoflex nanocomposite thin film was used as a flexible electrode layer. First, CNTs were dispersed in isopropyl alcohol (0.05 wt %) and spray-coated onto a donor substrate with a coating mask. After the removal of the coating mask, a prepolymer solution of the Ecoflex elastomer was poured onto the patterned CNT film. The Ecoflex prepolymer solution was then soaked into the patterned CNT network film to form a percolated structure. After the curing of the Ecoflex prepolymer solution in a convection oven at 60 °C for 1 h, a CNT−Ecoflex nanocomposite thin film as an electrode layer was formed by peeling it off from the donor substrate.

Characterization of Porous Ecoflex and CNT−Ecoflex Nanocomposite Film. The surface and cross-sectional morphologies of the porous Ecoflex layer and the CNT−Ecoflex nanocomposite film were characterized by optical microscopy (Digital Microscope, VHX-1000, Keyence, Osaka, Japan) and by field-emission scanning electron microscopy (FE-SEM, Sirion, FEI, Hillsboro, OR, USA). The internal structure of the porous Ecoflex layer was nondestructively visualized by high-resolution microcomputed tomography (Micro-CT, SkyScan

DOI: 10.1021/acsami.6b04225
ACS Appl. Mater. Interfaces 2016, 8, 16922−16931

1272, Bruker AXS, Fitchburg, WI, USA). The porosity was calculated by considering the mass ratio between solid and porous Ecoflex blocks with identical dimensions. The current−voltage (I−V) characteristics of the CNT−Ecoflex nanocomposite film were determined using a semiconductor parameter analyzer (4155A, HP, Palo Alto, CA, USA).

Characterization of Sensor Response. A high-precision universal testing machine (INSTRON 5965, INSTRON, Norwood, MA, USA) was employed to characterize the sensing performances of the fabricated sensors. A disk-type compression fixture with a diameter of 40 mm was utilized for uniform deformation of the sensor. A position-controlled compression test was conducted at a constant speed of 0.2 mm s^{-1} (0.17 μm position resolution). The force was recorded with a force transducer (INSTRON 2580-106, INSTRON) which ensures ±0.5% accuracy of the readout value with a maximum load capacity of 1 kN. The capacitance of each sensor was measured with a precision LCR meter (E4980A, Agilent, Santa Clara, CA, USA) at a frequency of 400 kHz.

RESULTS AND DISCUSSION

Figure 1 describes the working principle of the proposed piezocapacitive sensor based on a 3-D microporous elastomeric dielectric layer compared to a conventional solid (i.e., nonporous) dielectric layer. The capacitance value of the parallel-plate capacitor is determined by the dielectric constant (ε_r), the area of the overlapped electrodes (A), and the distance between the two electrodes (d). Schematic illustrations representing the compressive behaviors of the pressure sensors using solid and porous elastomeric dielectric layers upon identical amounts of pressure input are shown in Figure 1a,b, respectively. Additionally, a graphical explanation for the capacitance responses of the sensors to identical levels of external pressure according to the compressive behaviors of solid and porous elastomeric dielectric layers is provided in Figure 1c as well. Conventional sensors based on a solid elastomeric dielectric layer undergo the barreling phenomenon under compression. Thus, the change of d (Δd_s) is the most dominant factor with regard to capacitance changes upon loading. On the other hand, compared to conventional sensors, a sensor using a porous elastomeric dielectric layer is deformed by a much larger amount ($\Delta d_p > \Delta d_s$) owing to the reduced stiffness. Thus, a much larger capacitance change can be induced upon an identical pressure input. Furthermore, the capacitance change can be further boosted by the increase of the effective dielectric constant with gradual closure of the micropores under external pressure ($\Delta \varepsilon_p > \Delta \varepsilon_s \sim 0$). The combination of large deformation and an increase in the effective dielectric constant of the porous dielectric material enables a significant increase of the sensitivity. During the unloading process, the elastic restoring force of the elastomer fraction allows the reopening of closed pores, consequently allowing the porous structure to return to its initial state and leading to the perfect recovery of the sensor response. Therefore, a highly sensitive response can be achieved by using a porous elastomeric dielectric layer based on its reduced stiffness and the increased effective dielectric constant of the porous elastomeric dielectric layer. In addition to the high sensitivity, the barreling phenomenon can be inhibited by providing sufficient void spaces that can be replaced with neighboring elastomeric structures, leading to superior stability of the sensor structure under high compression levels. This barreling phenomenon can become a critical problem in the compact packaging of sensor arrays with high spatial resolutions, as the adjacent sensors can undergo interference due to the lateral expansion of the compressed dielectric layer. Therefore, adoption of a porous elastomeric dielectric layer can also provide an advantage of developing a high spatial resolution pressure mapping sensor array.

A schematic diagram of the proposed pressure sensor is illustrated in Figure 2a. The piezocapacitive-type pressure

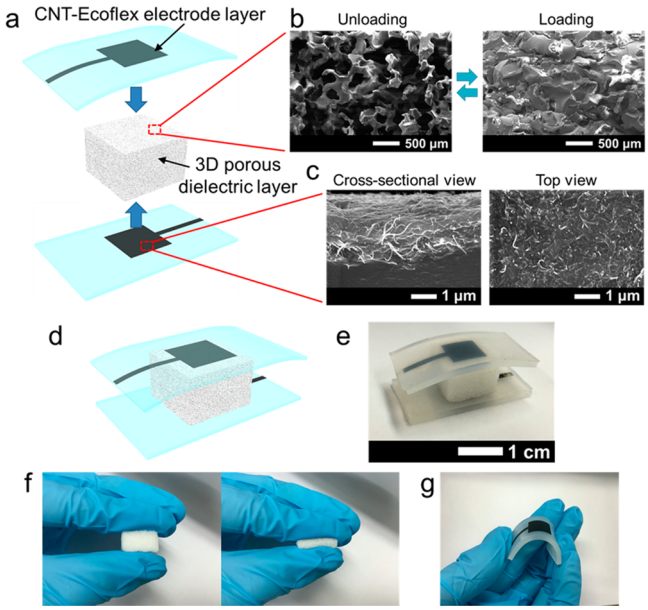

Figure 2. Design of the flexible piezocapacitive pressure sensor. (a) Schematic diagram of a flexible piezocapacitive pressure sensor consisting of CNT−Ecoflex nanocomposite film electrode layers and a microporous Ecoflex dielectric layer between them. (b) SEM images of the porous Ecoflex dielectric layer before and after being compressed. (c) SEM images of the CNT−Ecoflex nanocomposite film electrode layer. (d) Fabrication of the sensor by stacking components with a careful alignment. (e) Photograph of the overall sensor structure. (f) Flexibility of the porous elastomeric dielectric layer. (g) Flexibility of the CNT−Ecoflex nanocomposite film electrode layer.

sensor consists of two flexible parallel electrode layers and a 3-D microporous dielectric layer between them. For the dielectric layer, we adopted a 3-D microporous elastomer structure possessing randomly distributed micropores throughout the entire volume. The microporous structure was formed by casting a platinum-catalyzed silicone (Ecoflex) prepolymer solution within a sugar cube template (see the Experimental Section for details). The cross-sectional morphologies of the microporous Ecoflex layer in loading/unloading states were characterized by scanning electron microscopy (SEM) (Figure 2b). The size of the micropores was observed to be 288 ± 85 μm, and the porosity was calculated as 62.8 ± 0.7%. Moreover, the consistency of the microporous configuration of the dielectric layer within the entire volume was confirmed by microcomputed tomography (Figure S1 and Movie S1, Supporting Information). Originally, solid Ecoflex is one of the most flexible elastomeric materials, with compliance levels similar to that of human skin. By introducing micropores, the compressibility of the porous Ecoflex was increased significantly by ~20 times as compared to solid Ecoflex, which is critical for sensitive piezocapacitive pressure sensing (Figure S2, Supporting Information). For the electrode layers, CNT−Ecoflex nanocomposite thin film was used as a conducting material with a square-shaped electrode pattern. As shown in Figure 2c, the

DOI: 10.1021/acsami.6b04225
ACS Appl. Mater. Interfaces 2016, 8, 16922−16931

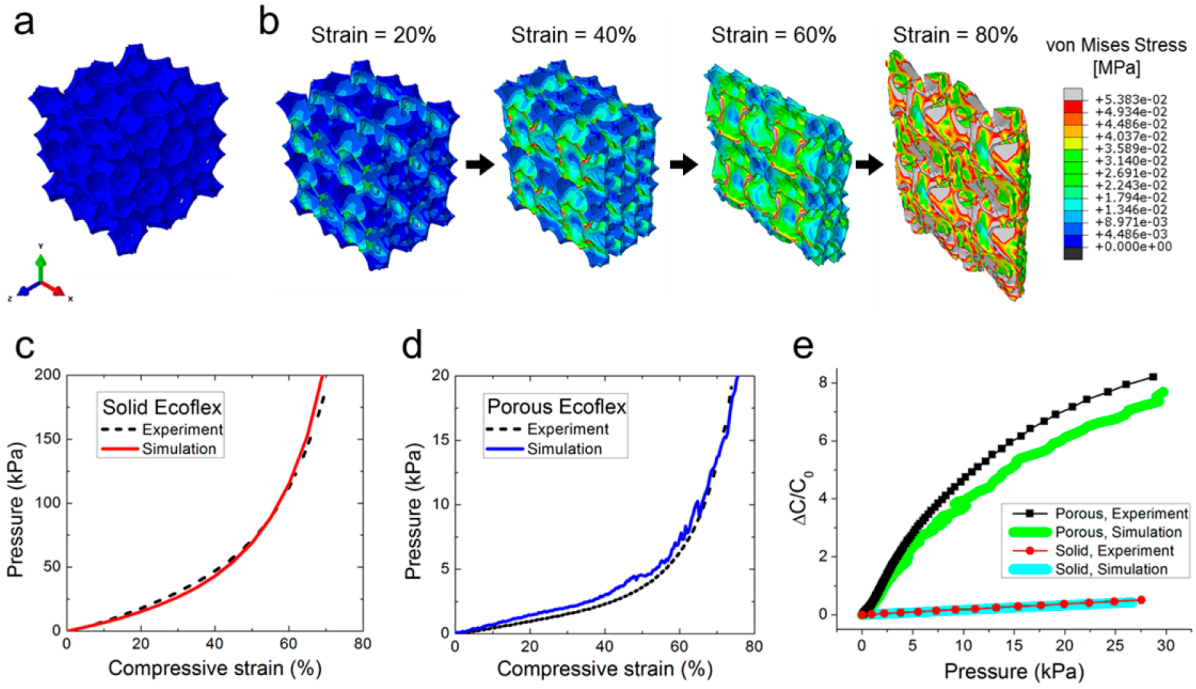

Figure 3. FE simulations to investigate the compressive behavior of solid and microporous Ecoflex dielectric cubes. (a) Full 3-D representative model of the porous Ecoflex dielectric cube. (b) Gradual compressive behavior of the representative model of the porous Ecoflex dielectric cube in panel a. (c) Compressive strain−pressure curves of the solid Ecoflex cube by experiment and simulation. (d) Compressive strain−pressure curves of the porous Ecoflex cube by experiment and simulation. (e) Plot of the relative capacitance changes in response to external pressure by experiment and simulation for parallel-plate capacitor models with solid and microporous Ecoflex dielectric layers.

CNT network was embedded in the Ecoflex layer while the CNTs remained in contact, leading to an electrical conductivity of 340.22 S/m, as calculated from the current−voltage characteristics of the CNT−Ecoflex nanocomposite thin film (Figure S3, Supporting Information). Originally, pristine CNT network films coated onto an arbitrary substrate can easily be broken by external friction. However, the CNT−Ecoflex nanocomposite film can provide robust percolated structures, ensuring both good conductivity and flexibility. The sensor components were stacked by the careful alignment of two patterned electrodes with a porous dielectric layer, as shown in Figure 2d. A photograph of the overall sensor structure is displayed in Figure 2e. Such fabricated sensors have flexible and bendable components with extremely high compressibility of the porous elastomer (Figure 2f,g).

For an in-depth investigation of the sensing mechanism of the piezocapacitive pressure sensor, we modeled the compressive behavior of the dielectric layer using finite element (FE) analysis, as shown in Figure 3. The material properties of the solid Ecoflex were initially measured through a compression test up to a compressive engineering strain of $\varepsilon = 0.7$, as shown in Figure 3c (the black dotted line). The nonlinear constitutive behavior was accurately captured by the Neo-Hookean hyperelastic model (the red solid line in Figure 3c). Details about the constitutive model and the identified material constants can be found in the Supporting Information. To simulate the compressive behavior of the porous Ecoflex cube in the FE framework, its complex random geometry was considered as a periodic structure in the 3-D coordinate space. Owing to the complicated contact conditions within the porous media, we performed simulations using the commercial FE code ABAQUS/Explicit while ensuring that the kinetic energy contribution remained insignificant (i.e., less than 0.1%). Details about the implementation of the periodic boundary condition in the FE framework can be found in the Supporting Information. A cubic unit cell (1 mm × 1 mm × 1 mm) for the porous Ecoflex cube was modeled to represent the critical features of the cube (e.g., the porosity, pore size, and their distributions). Specifically, nine different spheres were randomly generated based on the experimentally obtained pore information (i.e., pore size = 288 ± 85 μm and porosity = 62.8%). These nine spheres were then subtracted at the body-centered cubic (BCC) lattice points of an eighth of a cubic solid unit cell, generating an eighth of a porous unit cell. The subtracted eighth of the porous unit cell was then employed to assemble a full porous unit cell (i.e., the simulation model shown in Figure 3a as a representative model), in which periodic boundary conditions were applied.[45] Full 3-D models were constructed using four-node tetrahedral elements (i.e., C3D4 in ABAQUS/Explicit), and a sweeping mesh size of 0.05 mm was employed to ensure the convergence of the FE simulations. By changing the combination of the radius of subtracting nine spheres, a few different simulation models were constructed, resulting in similar compressive behavior. The gradual compressive behavior from a representative unit cell is shown in Figure 3b. A numerically calculated compressive strain−pressure curve shows excellent agreement with the experimentally measured data (Figure 3d). Furthermore, we calculated the capacitance responses to external pressure and compressive strain as generated from the FE simulation results using parallel-plate capacitor models with a solid Ecoflex dielectric layer and a porous Ecoflex dielectric layer. Details about the analytic model and the modeling assumptions are found in the Supporting Information. As shown in Figure 3e, there is a good match between the experimental data and the calculated values.

DOI: 10.1021/acsami.6b04225
ACS Appl. Mater. Interfaces 2016, 8, 16922−16931

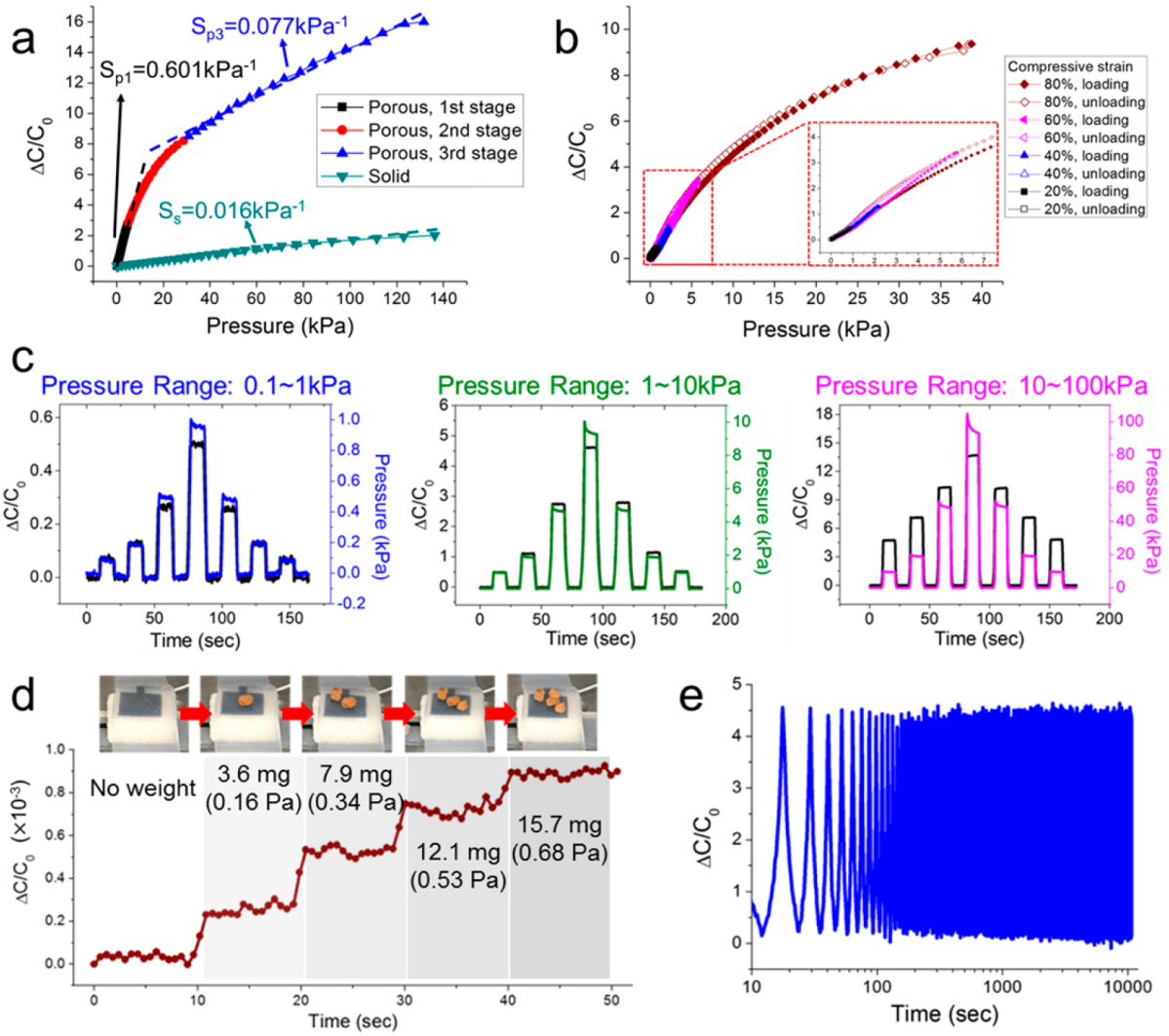

Figure 4. Pressure-sensing performance of the piezocapacitive pressure sensor with a microporous Ecoflex dielectric layer. (a) Pressure−response curves of the piezocapacitive pressure sensors using solid and microporous Ecoflex dielectric layers. (b) Hysteresis characteristics of the pressure sensor in response to different compression levels. (c) Dynamic responses of the pressure sensor at various pressures ranging from 0.1 to 100 kPa. (d) Demonstration of LOD by means of the sequential detection of ultralightweight objects, i.e., coffee powders in this case. (e) Stability of the pressure sensor over 1000 cycles of a repeated compression test.

Figure 4 displays the characteristics of the proposed sensor in the pressure range of 0−130 kPa. The pressure-sensing performance was examined by plotting the curves of the external pressure input (P) vs the relative change of the capacitance ($\Delta C/C_0$) for both porous and solid dielectric layers (Figure 4a). The sensitivity (S) is defined as the slope of the curve ($S = \delta(\Delta C/C_0)/\delta P$). The piezocapacitive sensor using the microporous Ecoflex dielectric layer showed three different stages with different compressive behaviors upon an increase in the pressure input. In the first stage up to a pressure level of 5 kPa (shown in black), excellent pressure-sensing performance resulted, with linear behavior and high sensitivity (S_{p1} = 0.601 kPa^{-1}, R^2 = 0.996; see Figure S4a, Supporting Information). It should be noted that the sensitivity of the sensor using the porous Ecoflex dielectric layer is nearly 37.6 times higher than that of the sensor using the solid Ecoflex dielectric layer. This highly sensitive pressure-sensing capability in the first stage originated from two factors: the significant compressibility of the microporous elastomeric dielectric layer and the simultaneous replacement of the air in pore fraction with the neighboring Ecoflex during compression. Specifically, the volume fraction of the micropores is large enough to create significant deformation of the dielectric layer as compared to a solid dielectric layer at under an identical pressure level, and this can produce a significant change of the capacitance. Moreover, the increase in the effective dielectric constant contributes to a further change of the capacitance as the air in the pores ($\varepsilon_r \sim 1.0$) is replaced with the neighboring Ecoflex structures ($\varepsilon_r \sim 2.5$) during the contraction process. In the second stage (pressure = 5−30 kPa, marked in red) shown in Figure 4a, the sensor response exhibited a gradual reduction of the sensitivity. This response was caused by the rise of the elastic resistance of the porous elastomer structure, as additional pressure continues to cram the buckled Ecoflex bridges into the pores. Moreover, the pores are gradually closed and the Ecoflex bridges form more contacts between them. Therefore, further compression becomes more hindered by the mechanical strengthening of the porous Ecoflex network. In the third stage, which is above 30 kPa (the blue-colored region), the pores appeared to be completely closed such that the sensor

DOI: 10.1021/acsami.6b04225
ACS Appl. Mater. Interfaces 2016, 8, 16922−16931

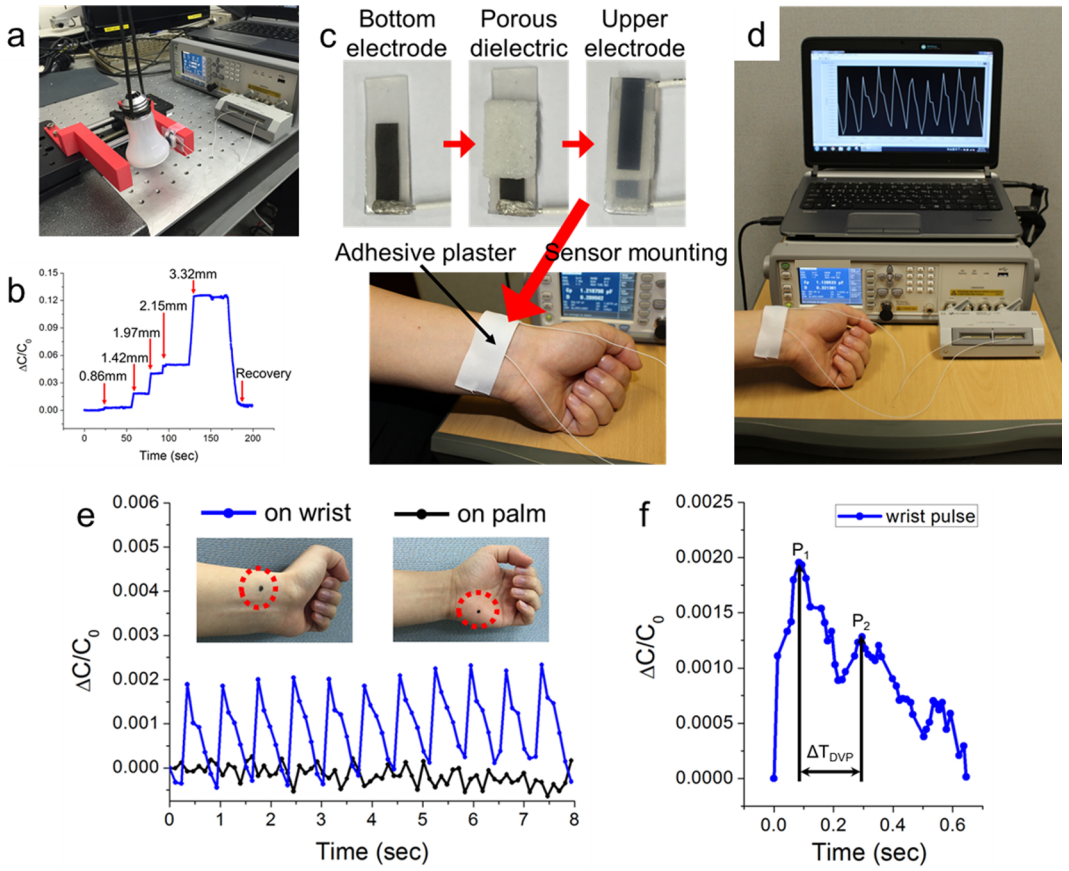

Figure 5. Applications of the piezocapacitive pressure sensor with the microporous Ecoflex dielectric layer to wearable pressure-sensing devices. (a) Robotic fingers integrated with the piezocapacitive sensor. (b) Capacitance responses at each displacement of one finger. (c) Mounting of the pressure sensor onto a human wrist with a commercial adhesive plaster. (d) Measurement setup for the real-time monitoring of human wrist pulse signals. (e) Capacitance responses of the sensor on the wrist and the palm. (f) High-speed measurement of a typical single wrist pulse, indicating two peaks, P_1 and P_2.

showed solid-like behavior with low but stable sensitivity (S_{p3} = 0.077 kPa^{-1}, R^2 = 0.989) over a very wide pressure span of 30−130 kPa (Figure S4b, Supporting Information). Although the sensitivity of the third stage is lower than that of the first stage, it should also be noted that the sensitivity over a very wide pressure span of 30−130 kPa is still ∼4.8 times higher than that of the sensor using the solid Ecoflex dielectric layer.

Previous studies commonly have been associated with dramatic decreases of the sensitivity or no sensitivity after a narrow dynamic range of approximately 10 kPa despite their high sensitivities in low-pressure regimes (Figure S5a, Supporting Information).[19,22,37−40,43,46,47] However, our sensor, based on a porous elastomeric dielectric layer, could provide a wide dynamic range up to 130 kPa without a significant drop in the sensitivity. Moreover, for actual applications, decreased sensitivity at a higher pressure regime is not a serious disadvantage, as a high-pressure regime does not require as a high resolution as in a low-pressure regime. This can be confirmed by the log−linear plot of the pressure vs the response (pressure on the log scale and response on the linear scale), indicating similar resolutions in each pressure regime (Figure S6). These observations of the pressure-sensing performance indicate that our sensor is suitable for practical human tactile pressure sensing.

In addition, the sensor showed negligible hysteresis at various pressure levels up to a compressive strain of 80% (Figure 4b). We observed perfectly reversible closure/opening behavior of micropores with the buckling/releasing of Ecoflex bridges within the microporous Ecoflex network (Movie S2, Supporting Information). Because the existence of pores could contribute to the reduction of the viscoelastic property of the bulk Ecoflex, a reversible sensor response could be achieved without noticeable hysteresis. As shown in Figure 4c, we also observed that our sensor produces an excellent match between the pressure input profile and the response curve with continuous, stable, noise-free and perfectly reversible signals through dynamic testing at various pressures ranging from 0 to 100 kPa. We also examined the limit of detection (LOD) of the proposed sensor, as shown in Figure 4d. The LOD is an important parameter for the realization of ultralow-force detection capabilities, such as the monitoring of air flows, sound waves, and the propagation of small mechanical vibrations.[15] Sequential detection of an ultralightweight object was demonstrated using small coffee powders with a mass of ∼4 mg, corresponding to a pressure level of 0.1−0.2 Pa. To the best of our knowledge, this is the first demonstration of the sequential detection of an ultralightweight object with the lowest limit of detection among previous achievements (Figure S5b, Supporting Information).[19,22,37−40,43,46,47] As explained previously, due to the combined effect of the ultrahigh compliance of porous Ecoflex and the increased effective dielectric constant, our sensor offers extremely high sensitivity to low pressures. In addition, the reliability of our sensor was evaluated by applying 1000 repeated compression/release

DOI: 10.1021/acsami.6b04225
ACS Appl. Mater. Interfaces 2016, 8, 16922−16931

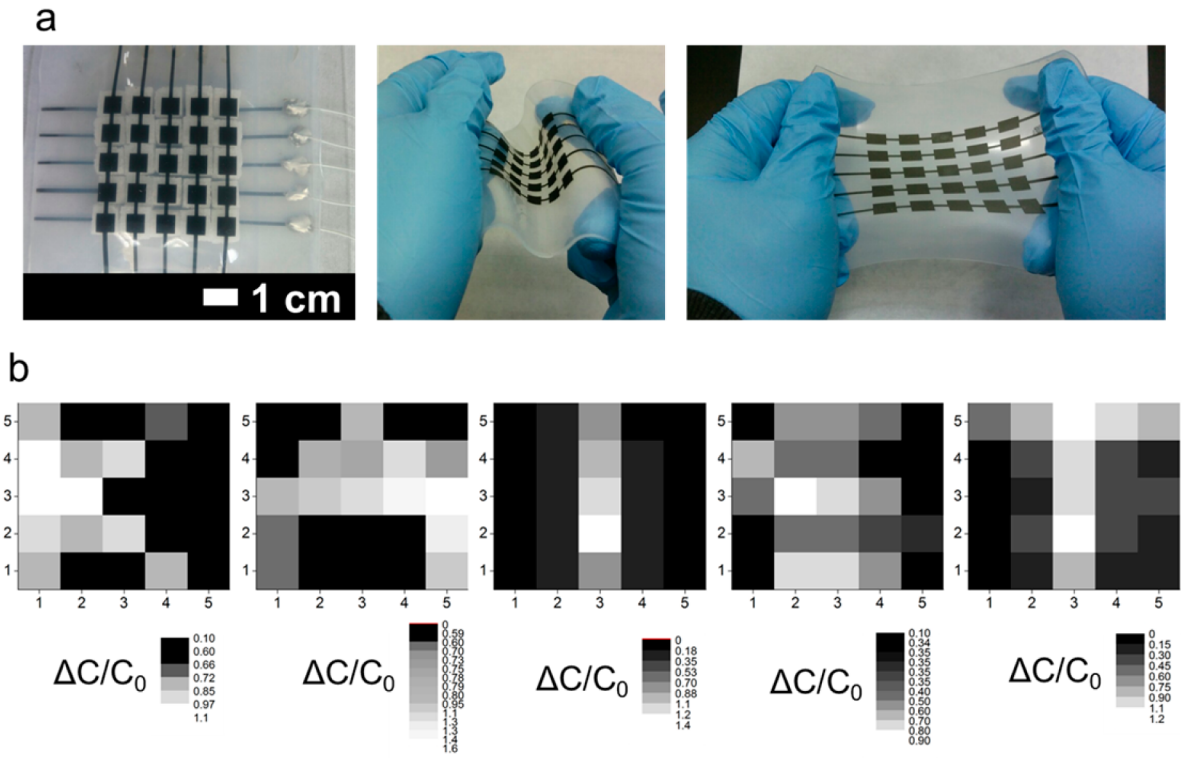

Figure 6. Application of the piezocapacitive pressure sensor with the microporous Ecoflex dielectric layer to a flexible pressure sensor array pad for the detection of spatial pressure distributions in two-dimensional space. (a) Fabricated flexible pressure sensor array pad with 5 × 5 pixels of flexible and stretchable electrode layers. (b) Recognition of the pressure distribution on the pressure sensor array pad by applying stamps patterned with the letters "K", "A", "I", "S", and "T".

cycles (between the minimum pressure of 0.45 kPa and the maximum pressure of 13 kPa) to the sensor in order to investigate its long-term stability and mechanical durability (Figure 4e). No drift of the sensor response and no structural change of the microporous Ecoflex network were found during the 1000 compression/release cycles. Finally, the reproducibility of our sensors for commercialization was verified by comparing 10 different samples. Given that the dielectric layer of our sensor was fabricated by casting a liquid precursor of Ecoflex into a sugar cube template, it is important to check if all sensors made with different sugar cube templates exhibit consistent responses. Thus, we fabricated 10 sensor samples made from different sugar cubes and compared their capacitance responses. It was observed that these 10 sensor samples showed nearly identical initial values (C_0 = 141.50 ± 1.06 fF) as well as capacitance changes at identical pressures (Figure S7, Supporting Information). Although micropores with an irregular size were randomly distributed within the volume of the porous Ecoflex dielectric layer, we confirmed that the sensor using the porous Ecoflex dielectric layer could feasibly represent consistent mechanical and electrical behavior in the macroscale regime.

For a deeper investigation of the applicability of our sensor to wearable pressure-sensing devices, it was employed as (i) an electronic pressure-sensing skin to determine seizing force levels in robotic fingers and (ii) as a bandage-type pressure-sensing device for the detection of a human wrist pulse signals. In the first example, our sensor was integrated onto robotic finger tips so that the fingers could recognize the pressure level that was subjected through contact with a target object. Figure 5a shows a photograph of the fabricated robotic fingers and a lightbulb as the target object. The seizing motion was performed using a linear moving stage operated by a stepper motor. The capacitance responses successfully reflected the random seizing motions applied in sequence, showing perfect signal recovery, as depicted in Figure 5b. Moreover, the microporous elastomer structure functions as a shock absorber, similar to the cushion of human skin surrounding the human skeleton. Thus, the robotic finger with flexible sensor skin could handle fragile objects such as a lightbulb without breaking them.

In the second example, a wearable real-time wrist-pulse-sensing device was demonstrated. As shown in Figure 5c, the wrist-pulse-sensing device was fabricated by stacking the sensor components, and it was mounted directly onto the human wrist skin with commercial medical adhesive plaster. The real-time measurement setup is shown in Figure 5d. The wrist pulse signal was clearly detected by our sensor in real time (~90 beats/min), as shown in Movie S3 in the Supporting Information. To verify whether the sensor signal truly came from the deflection of human skin induced by the wrist pulse, we compared the sensor signal on the wrist with that on the palm, where there is no skin deflection induced by a bloodstream. As shown in Figure 5e, the sensor signal on the wrist was clearly identified as compared to the noise level from the sensor attached on the palm. Furthermore, general clinical information as a measure of the arterial stiffness, which relates to the age of people, could also be collected and identified from the radial artery pressure wave measured by our sensor in the high-speed measurement setup mode (Figure 5f). Two clearly distinguishable peaks (P_1 and P_2) were obtained, which could be used to estimate clinical parameters; the radial artery augmentation index ($AI_r = P_2/P_1$) and the time between $P_1(t_1)$ and $P_2(t_2)$ of the digital volume pulse ($\Delta T_{DVP} = t_2 - t_1$) were

DOI: 10.1021/acsami.6b04225
ACS Appl. Mater. Interfaces 2016, 8, 16922−16931

measured and found to be 0.656 and 212 ms, respectively. These results are in good agreement with the reference data, which are comparable with the values expected for a healthy adult male in his late twenties.[29,48] In addition, the pressure induced from the pulse to the sensor at P_1 was estimated to be ~3 Pa, which was similar to the induced pressure measured by other wearable flexible wrist-pulse-sensing devices.[22,29]

Finally, a sensor array pad was fabricated using multiple porous elastomeric dielectric materials for the detection of spatially distributed pressures in a 2-D space. A flexible sensor array pad with a 5 × 5 pixel design was fabricated, as shown in Figure 6a. Stamps patterned with different letters of our institution, "KAIST," were then applied to the sensor array pad. Each letter was successfully recognized by the proposed sensor array pad, as shown in Figure 6b. As noted above, the microporous elastomeric dielectric layer does not produce the barreling phenomena, allowing the influence of neighboring sensor cells to be ignored.

CONCLUSION

In summary, we have developed a flexible piezocapacitive-type pressure sensor with ultrahigh sensitivity and stability over a wide dynamic range based on a porous elastomeric dielectric material via a facile and cost-effective process. By the presence of micropores within the elastomeric dielectric layer, our piezocapacitive-type pressure sensor is highly deformable by even very small pressure input levels, leading to a dramatic increase in its sensitivity. Moreover, the gradual closure of micropores under compression increases the effective dielectric constant, thereby further enhancing the sensitivity of the sensor. In addition, the 3-D microporous dielectric layer with serially stacked springs of Ecoflex bridges can cover a much wider pressure range than those of previously reported microstructured active materials. Accordingly, our pressure sensor showed excellent performance with ultrahigh sensitivity of 0.601 kPa^{-1} in a low-pressure regime (<5 kPa) as well as a wide dynamic range of 0.1 Pa to 130 kPa, which is appropriate for general tactile pressure ranges without a significant loss of sensitivity. To investigate its applicability to wearable devices, we demonstrated that our sensor can be easily utilized as a wearable pressure-sensing device in the form of (i) a pressure-sensing skin for seizing force measurements of robotic fingers and (ii) as a bandage-type wrist-pulse-monitoring device. Finally, a sensor array pad was fabricated for the detection of spatially distributed pressures, letter recognition in this case. We believe that the piezocapacitive pressure sensor based on the 3-D porous elastomeric dielectric layer can broaden our perspectives on applicable fields, such as the development of flexible microbalances, electronic skins for soft robotics, and wearable pressure-sensing devices for health diagnosis systems which deal with a wide pressure range from ultralow-pressure touch to human tactile pressure.

ASSOCIATED CONTENT

Supporting Information

The Supporting Information is available free of charge on the ACS Publications website at DOI: 10.1021/acsami.6b04225.

Finite element (FE) analysis of the compressive behavior of the microporous Ecoflex cube, analytical model of the capacitor with the composite dielectric layer (PDF)

Microcomputed tomography movie the microporous configuration of the dielectric layer within the entire volume (AVI)

Reversible closure/opening behavior of micropores with the buckling/releasing of Ecoflex bridges within the microporous Ecoflex network (AVI)

Detection of wrist pulse signal with sensor in real time (AVI)

AUTHOR INFORMATION

Corresponding Author

*E-mail: inkyu@kaist.ac.kr.

Notes

The authors declare no competing financial interest.

ACKNOWLEDGMENTS

This work was supported by the following research grants: (1) Industrial Strategic Technology Development Program (No. 10041618, Development of Needle Insertion Type Image-based Interventional Robotic System for Biopsy and Treatment of 1 cm Abdominal and Thoracic Lesion with Reduced Radiation Exposure and Improved Accuracy) funded by the Ministry of Trade Industry and Energy (MI, Korea) and the Brain Korea 21 Project in 2014; (2) National Research Foundation of Korea (NRF) grant funded by the Korean Government (MSIP) (No. 2015R1A5A1037668); and (3) Fundamental Research Program (Grant PNK3771) of the Korean Institute of Materials Science (KIMS)

REFERENCES

(1) Someya, T.; Sekitani, T.; Iba, S.; Kato, Y.; Kawaguchi, H.; Sakurai, T. A Large-Area, Flexible Pressure Sensor Matrix with Organic Field-Effect Transistors for Artificial Skin Applications. *Proc. Natl. Acad. Sci. U. S. A.* **2004**, *101*, 9966−9970.

(2) Wang, C.; Hwang, D.; Yu, Z.; Takei, K.; Park, J.; Chen, T.; Ma, B.; Javey, A. User-Interactive Electronic Skin for Instantaneous Pressure Visualization. *Nat. Mater.* **2013**, *12*, 899−904.

(3) Hammock, M. L.; Chortos, A.; Tee, B. C. K.; Tok, J. B. H.; Bao, Z. 25th Anniversary Article: The Evolution of Electronic Skin (E-Skin): A Brief History, Design Considerations, and Recent Progress. *Adv. Mater.* **2013**, *25*, 5997−6038.

(4) Wang, X.; Dong, L.; Zhang, H.; Yu, R.; Pan, C.; Wang, Z. L. Recent Progress in Electronic Skin. *Adv. Sci.* **2015**, *2*, 1500169.

(5) Cherenack, K.; Zysset, C.; Kinkeldei, T.; Münzenrieder, N.; Tröster, G. Woven Electronic Fibers with Sensing and Display Functions for Smart Textiles. *Adv. Mater.* **2010**, *22*, 5178−5182.

(6) Stoppa, M.; Chiolerio, A. Wearable Electronics and Smart Textiles: a Critical Review. *Sensors* **2014**, *14*, 11957−11992.

(7) Lee, J.; Kwon, H.; Seo, J.; Shin, S.; Koo, J. H.; Pang, C.; Son, S.; Kim, J. H.; Jang, Y. H.; Kim, D. E.; Lee, T. Conductive Fiber-Based Ultrasensitive Textile Pressure Sensor for Wearable Electronics. *Adv. Mater.* **2015**, *27*, 2433−2439.

(8) Lipomi, D. J.; Vosgueritchian, M.; Tee, B. C.; Hellstrom, S. L.; Lee, J. A.; Fox, C. H.; Bao, Z. Skin-Like Pressure and Strain Sensors Based on Transparent Elastic Films of Carbon Nanotubes. *Nat. Nanotechnol.* **2011**, *6*, 788−792.

(9) Fan, F. R.; Lin, L.; Zhu, G.; Wu, W.; Zhang, R.; Wang, Z. L. Transparent Triboelectric Nanogenerators and Self-Powered Pressure Sensors Based on Micropatterned Plastic Films. *Nano Lett.* **2012**, *12*, 3109−3114.

(10) Trivedi, D.; Rahn, C. D.; Kier, W. M.; Walker, I. D. Soft Robotics: Biological Inspiration, State of the Art, and Future Research. *Appl. Bion. Biomech.* **2008**, *5*, 99−117.

(11) Pfeifer, R.; Lungarella, M.; Iida, F. The Challenges Ahead for Bio-Inspired 'Soft' Robotics. *Commun. ACM* **2012**, *55*, 76−87.

DOI: 10.1021/acsami.6b04225
ACS Appl. Mater. Interfaces 2016, 8, 16922−16931

(12) Bauer, S.; Bauer-Gogonea, S.; Graz, I.; Kaltenbrunner, M.; Keplinger, C.; Schwodiauer, R. 25th Anniversary Article: a Soft Future: from Robots and Sensor Skin to Energy Harvesters. *Adv. Mater.* **2014**, *26*, 149−161.
(13) Kim, J.; Lee, M.; Shim, H. J.; Ghaffari, R.; Cho, H. R.; Son, D.; Jung, Y. H.; Soh, M.; Choi, C.; Jung, S.; Chu, K.; Jeon, D.; Lee, S. T.; Kim, J. H.; Choi, S. H.; Hyeon, T.; Kim, D. H. Stretchable Silicon Nanoribbon Electronics for Skin Prosthesis. *Nat. Commun.* **2014**, *5*, 5747.
(14) Boutry, C. M.; Nguyen, A.; Lawal, Q. O.; Chortos, A.; Rondeau-Gagne, S.; Bao, Z. A Sensitive and Biodegradable Pressure Sensor Array for Cardiovascular Monitoring. *Adv. Mater.* **2015**, *27*, 6954−6961.
(15) Zang, Y.; Zhang, F.; Di, C.-a.; Zhu, D. Advances of Flexible Pressure Sensors toward Artificial Intelligence and Health Care Applications. *Mater. Horiz.* **2015**, *2*, 140−156.
(16) Yang, Y.; Zhang, H.; Lin, Z.-H.; Zhou, Y. S.; Jing, Q.; Su, Y.; Yang, J.; Chen, J.; Hu, C.; Wang, Z. L. Human Skin Based Triboelectric Nanogenerators for Harvesting Biomechanical Energy and as Self-Powered Active Tactile Sensor System. *ACS Nano* **2013**, *7*, 9213−9222.
(17) Zhu, G.; Yang, W. Q.; Zhang, T.; Jing, Q.; Chen, J.; Zhou, Y. S.; Bai, P.; Wang, Z. L. Self-Powered, Ultrasensitive, Flexible Tactile Sensors Based on Contact Electrification. *Nano Lett.* **2014**, *14*, 3208−3213.
(18) Wang, S.; Lin, L.; Wang, Z. L. Triboelectric Nanogenerators as Self-Powered Active Sensors. *Nano Energy* **2015**, *11*, 436−462.
(19) Mannsfeld, S. C.; Tee, B. C.; Stoltenberg, R. M.; Chen, C. V.; Barman, S.; Muir, B. V.; Sokolov, A. N.; Reese, C.; Bao, Z. Highly Sensitive Flexible Pressure Sensors with Microstructured Rubber Dielectric Layers. *Nat. Mater.* **2010**, *9*, 859−864.
(20) Hu, C.-F.; Su, W.-S.; Fang, W. Development of Patterned Carbon Nanotubes on a 3D Polymer Substrate for the Flexible Tactile Sensor Application. *J. Micromech. Microeng.* **2011**, *21*, 115012.
(21) Tee, B. C. K.; Wang, C.; Allen, R.; Bao, Z. An Electrically and Mechanically Self-Healing Composite with Pressure- and Flexion-Sensitive Properties for Electronic Skin Applications. *Nat. Nanotechnol.* **2012**, *7*, 825−832.
(22) Gong, S.; Schwalb, W.; Wang, Y.; Chen, Y.; Tang, Y.; Si, J.; Shirinzadeh, B.; Cheng, W. A Wearable and Highly Sensitive Pressure Sensor with Ultrathin Gold Nanowires. *Nat. Commun.* **2014**, *5*, 3132.
(23) Lee, J.; Kim, S.; Lee, J.; Yang, D.; Park, B. C.; Ryu, S.; Park, I. A Stretchable Strain Sensor Based on a Metal Nanoparticle Thin Film for Human Motion Detection. *Nanoscale* **2014**, *6*, 11932−11939.
(24) Wang, X.; Li, T.; Adams, J.; Yang, J. Transparent, Stretchable, Carbon-Nanotube-Inlaid Conductors Enabled by Standard Replication Technology for Capacitive Pressure, Strain and Touch sensors. *J. Mater. Chem. A* **2013**, *1*, 3580−3586.
(25) Yao, S.; Zhu, Y. Wearable Multifunctional Sensors using Printed Stretchable Conductors Made of Silver Nanowires. *Nanoscale* **2014**, *6*, 2345−2352.
(26) Woo, S.-J.; Kong, J.-H.; Kim, D.-G.; Kim, J.-M. A Thin All-Elastomeric Capacitive Pressure Sensor Array Based on Micro-Contact Printed Elastic Conductors. *J. Mater. Chem. C* **2014**, *2*, 4415−4422.
(27) Kim, S. Y.; Park, S.; Park, H. W.; Park, D. H.; Jeong, Y.; Kim, D. H. Highly Sensitive and Multimodal All-Carbon Skin Sensors Capable of Simultaneously Detecting Tactile and Biological Stimuli. *Adv. Mater.* **2015**, *27*, 4178−4185.
(28) Wang, Z. L.; Song, J. Piezoelectric Nanogenerators Based on Zinc Oxide Nanowire Arrays. *Science* **2006**, *312*, 242−246.
(29) Dagdeviren, C.; Su, Y.; Joe, P.; Yona, R.; Liu, Y.; Kim, Y.-S.; Huang, Y.; Damadoran, A. R.; Xia, J.; Martin, L. W.; Huang, Y.; Rogers, J. A. Conformable Amplified Lead Zirconate Titanate Sensors with Enhanced Piezoelectric Response for Cutaneous Pressure Monitoring. *Nat. Commun.* **2014**, *5*, 4496.
(30) Pan, C.; Dong, L.; Zhu, G.; Niu, S.; Yu, R.; Yang, Q.; Liu, Y.; Wang, Z. L. High-Resolution Electroluminescent Imaging of Pressure Distribution using a Piezoelectric Nanowire LED Array. *Nat. Photonics* **2013**, *7*, 752−758.
(31) Ramuz, M.; Tee, B. C.; Tok, J. B.; Bao, Z. Transparent, Optical, Pressure-Sensitive Artificial Skin for Large-Area Stretchable Electronics. *Adv. Mater.* **2012**, *24*, 3223−3227.
(32) Yun, S.; Park, S.; Park, B.; Kim, Y.; Park, S. K.; Nam, S.; Kyung, K. U. Polymer-Waveguide-Based Flexible Tactile Sensor Array for Dynamic Response. *Adv. Mater.* **2014**, *26*, 4474−4480.
(33) Metzger, C.; Fleisch, E.; Meyer, J.; Dansachmüller, M.; Graz, I.; Kaltenbrunner, M.; Keplinger, C.; Schwödiauer, R.; Bauer, S. Flexible-Foam-Based Capacitive Sensor Arrays for Object Detection at Low Cost. *Appl. Phys. Lett.* **2008**, *92*, 013506.
(34) Tee, B. C. K.; Chortos, A.; Dunn, R. R.; Schwartz, G.; Eason, E.; Bao, Z. Tunable Flexible Pressure Sensors using Microstructured Elastomer Geometries for Intuitive Electronics. *Adv. Funct. Mater.* **2014**, *24*, 5427−5434.
(35) Pang, C.; Koo, J. H.; Nguyen, A.; Caves, J. M.; Kim, M. G.; Chortos, A.; Kim, K.; Wang, P. J.; Tok, J. B.; Bao, Z. Highly Skin-Conformal Microhairy Sensor for Pulse Signal Amplification. *Adv. Mater.* **2015**, *27*, 634−640.
(36) Pang, C.; Lee, G. Y.; Kim, T. I.; Kim, S. M.; Kim, H. N.; Ahn, S. H.; Suh, K. Y. A Flexible and Highly Sensitive Strain-Gauge Sensor using Reversible Interlocking of Nanofibres. *Nat. Mater.* **2012**, *11*, 795−801.
(37) Yao, H. B.; Ge, J.; Wang, C. F.; Wang, X.; Hu, W.; Zheng, Z. J.; Ni, Y.; Yu, S. H. A Flexible and Highly Pressure-Sensitive Graphene-Polyurethane Sponge Based on Fractured Microstructure Design. *Adv. Mater.* **2013**, *25*, 6692−6698.
(38) Choong, C. L.; Shim, M. B.; Lee, B. S.; Jeon, S.; Ko, D. S.; Kang, T. H.; Bae, J.; Lee, S. H.; Byun, K. E.; Im, J.; Jeong, Y. J.; Park, C. E.; Park, J. J.; Chung, U. I. Highly Stretchable Resistive Pressure Sensors using a Conductive Elastomeric Composite on a Micropyramid Array. *Adv. Mater.* **2014**, *26*, 3451−3458.
(39) Pan, L.; Chortos, A.; Yu, G.; Wang, Y.; Isaacson, S.; Allen, R.; Shi, Y.; Dauskardt, R.; Bao, Z. An Ultra-Sensitive Resistive Pressure Sensor Based on Hollow-Sphere Microstructure Induced Elasticity in Conducting Polymer Film. *Nat. Commun.* **2014**, *5*, 3002.
(40) Wang, X.; Gu, Y.; Xiong, Z.; Cui, Z.; Zhang, T. Silk-Molded Flexible, Ultrasensitive, and Highly Stable Electronic Skin for Monitoring Human Physiological Signals. *Adv. Mater.* **2014**, *26*, 1336−1342.
(41) Park, J.; Lee, Y.; Hong, J.; Lee, Y.; Ha, M.; Jung, Y.; Lim, H.; Kim, S. Y.; Ko, H. Tactile-Direction-Sensitive and Stretchable Electronic Skins Based on Human-Skin-Inspired Interlocked Microstructures. *ACS Nano* **2014**, *8*, 12020−12029.
(42) Su, B.; Gong, S.; Ma, Z.; Yap, L. W.; Cheng, W. Mimosa-Inspired Design of a Flexible Pressure Sensor with Touch Sensitivity. *Small* **2015**, *11*, 1886−1891.
(43) Tian, H.; Shu, Y.; Wang, X. F.; Mohammad, M. A.; Bie, Z.; Xie, Q. Y.; Li, C.; Mi, W. T.; Yang, Y.; Ren, T. L. A Graphene-Based Resistive Pressure Sensor with Record-High Sensitivity in a Wide Pressure Range. *Sci. Rep.* **2015**, *5*, 8603.
(44) Kwon, D.; Lee, T.-I.; Kim, M. S.; Kim, S.; Kim, T.-S.; Park, I. Porous Dielectric Elastomer Based Ultra-Sensitive Capacitive Pressure Sensor and Its Application to Wearable Sensing Device. *2015 Transducers—2015 18th International Conference on Solid-State Sensors, Actuators and Microsystems (TRANSDUCERS)*, Jun. 21−25, 2015; IEEE: New York, 2015; pp 299−302, DOI: 10.1109/TRANSDUCERS.2015.7180920.
(45) Shim, J.; Wang, P.; Bertoldi, K. Harnessing Instability-Induced Pattern Transformation to Design Tunable Photonic Crystals. *Int. J. Solids Struct.* **2015**, *58*, 52−61.
(46) Wu, W.; Wen, X.; Wang, Z. L. Taxel-Addressable Matrix of Vertical-Nanowire Piezotronic Transistors for Active and Adaptive Tactile Imaging. *Science* **2013**, *340*, 952−957.
(47) Schwartz, G.; Tee, B. C.-K.; Mei, J.; Appleton, A. L.; Kim, D. H.; Wang, H.; Bao, Z. Flexible Polymer Transistors with High Pressure Sensitivity for Application in Electronic Skin and Health Monitoring. *Nat. Commun.* **2013**, *4*, 1859.

DOI: 10.1021/acsami.6b04225
ACS Appl. Mater. Interfaces 2016, 8, 16922−16931

(48) Nichols, W. W. Clinical Measurement of Arterial Stiffness Obtained from Noninvasive Pressure Waveforms. *Am. J. Hypertens.* **2005**, *18*, 3S−10S.

DOI: 10.1021/acsami.6b04225
ACS Appl. Mater. Interfaces 2016, 8, 16922−16931

Supporting Information

Highly Sensitive, Flexible and Wearable Pressure Sensor Based on a Giant Piezocapacitive Effect of Three-Dimensional Microporous Elastomeric Dielectric Layer

Donguk Kwon,[a] Tae-Ik Lee,[a] Jongmin Shim,[b] Seunghwa Ryu,[a] Min Seong Kim,[a] Seunghwan Kim,[a] Taek-Soo Kim,[a] and Inkyu Park[,a,c]*

[a]Department of Mechanical Engineering, Korea Advanced Institute of Science and Technology (KAIST), 291 Daehak-ro, Yuseong-gu, Daejeon, 305-701, South Korea

[b]Department of Civil, Structural and Environmental Engineering, University at Buffalo, Buffalo, NY 14260, USA

[c]KI for the NanoCentury, Korea Advanced Institute of Science and Technology (KAIST), 291 Daehak-ro, Yuseong-gu, Daejeon, 305-701, South Korea

*E-mail: inkyu@kaist.ac.kr.

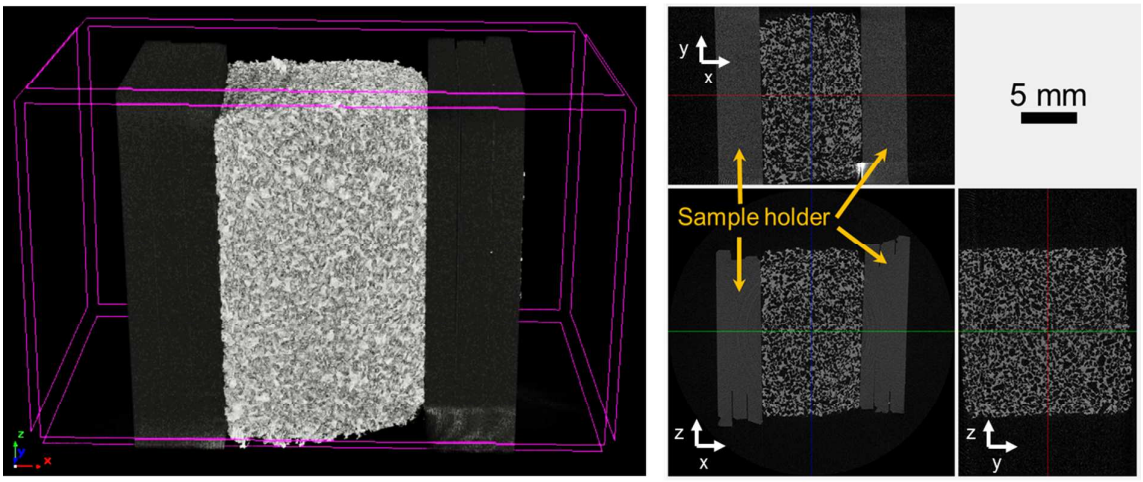

Figure S1. X-ray micro computed tomography (micro-CT) images showing internal microporous configuration within microporous Ecoflex dielectric layer taken from each axial direction of view.

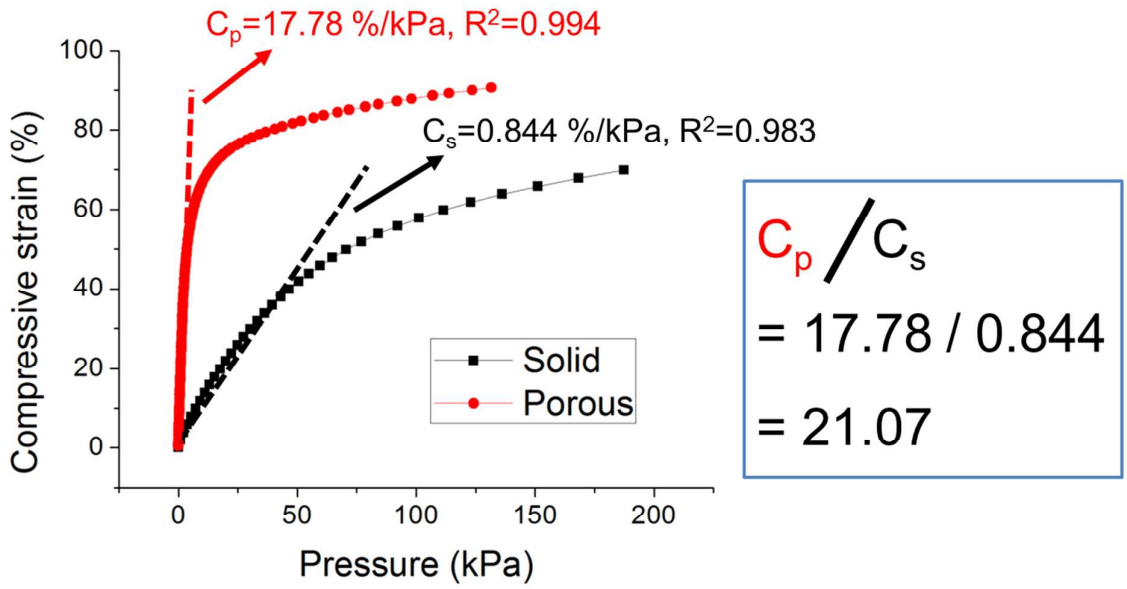

Figure S2. Compressive behaviors of the solid and microporous Ecoflex blocks. The compressibility was calculated as the slope of the curves up to the compressive strain of 40 %. The compressibility of microporous Ecoflex block was 17.78 %/kPa (R^2 = 0.994) while that of solid Ecoflex block was 0.844 %/kPa (R^2 = 0.983).

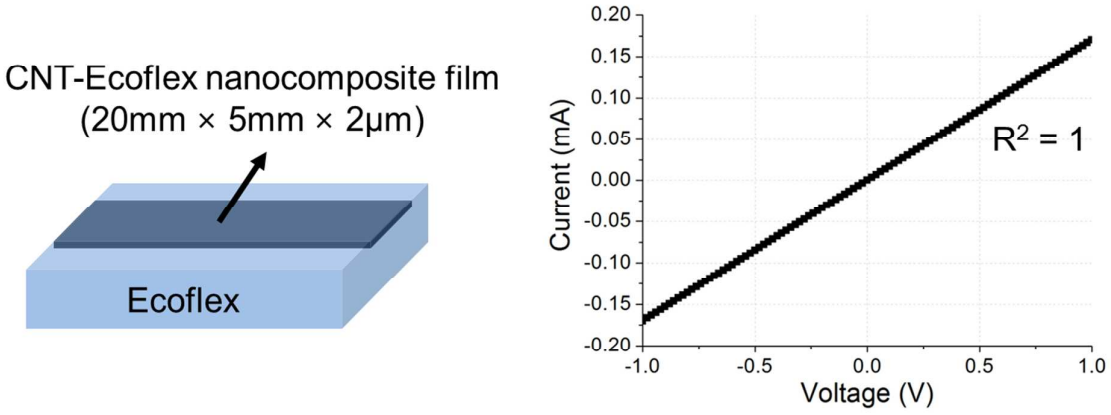

Figure S3. Schematic illustration of CNT-Ecoflex nanocomposite thin film and its current-voltage (I-V) characteristics showing metallic conductivity of 340.22 S/m.

Finite Element (FE) Analysis

To simulate the compressive behavior of the porous Ecoflex cube in the FE frame work, its constitutive behavior was described by a hyperelastic model and its complex random geometry was considered as a periodic structure. For the sake of the completeness of this article, this section briefly reviews the essentials for the employed constitutive model, the periodic boundary condition, and its implementation in the FE framework.

1) Constitutive Model

The nonlinear behavior of the solid Ecoflex was accurately described by the Neo-Hookean hyperelastic model,[1] whose strain energy function U is defined as:

$$U = \frac{G_0}{2}(\bar{I}_1 - 3) + \frac{K_0}{2}(J-1)^2 \tag{S1}$$

where G_0 and K_0 are material constants, $J = \det \boldsymbol{F}$ and $\bar{I}_1 = J^{-2/3}\mathrm{tr}(\boldsymbol{F}^T\boldsymbol{F})$, where $\boldsymbol{F}$ is the deformation gradient. Two Neo-Hookean constants $G_0 = 20\ kPa$ and $K_0 = 994\ kPa$ (red solid line in Figure 3c) are determined to capture the experimental behavior of the solid Ecoflex, and they are related to the initial Young's modulus E_0:

$$E_0 = \frac{9K_0G_0}{3K_0 + G_0}\ . \tag{S2}$$

2) Periodic Boundary Condition

For a given continuum body, we represent its undeformed and deformed configurations by Ω_0 and Ω. In addition, $\boldsymbol{X}$ and $\boldsymbol{x}$ denote material and spatial positions in Ω_0 and Ω, respectively. The deformation gradient of a motion in the body is defined as $\boldsymbol{F} = \partial \boldsymbol{x}/\partial \boldsymbol{X}$. In the 3-D coordinate space, the Bravais lattice for an infinitely periodic structure in the undeformed configuration is illustrated by a parallelepiped spanned by the material primitive lattice vectors $\boldsymbol{A}_j$ for $j = 1,2,3$.[2] Note that the application of macroscopic deformation gradient $\bar{\boldsymbol{F}}$ leads to a change in the primitive lattice vectors:[3]

$$\boldsymbol{a}_j = \bar{\boldsymbol{F}}\boldsymbol{A}_j \quad \text{for} \quad j = 1,2,3 \tag{S3}$$

where $\boldsymbol{a}_j$'s denote the spatial primitive lattice vectors.

To determine the static response of an infinite periodic structure subjected to a macroscopic deformation gradient $\bar{\boldsymbol{F}}$, the periodic displacement field $\boldsymbol{u}(\boldsymbol{x})$ needs to be represented by:[3]

$$\boldsymbol{u}(\boldsymbol{x}+\boldsymbol{r}) = \boldsymbol{u}(\boldsymbol{x}) + (\bar{\boldsymbol{F}} - \mathbf{1})\boldsymbol{R} \tag{S4}$$

where $\mathbf{1}$ denotes the third order identity tensor. In addition, $\boldsymbol{R}$ and $\boldsymbol{r}$ denote the material and the spatial lattice vector in the 3-D coordinate space, and they are described by:

$$\boldsymbol{r} = \sum_{j=1}^{3} r_j \boldsymbol{a}_j \quad , \qquad \boldsymbol{R} = \sum_{j=1}^{3} r_j \boldsymbol{A}_j = \bar{\boldsymbol{F}}\boldsymbol{r} \quad . \tag{S5}$$

For the case where no deformation is considered (i.e., $\bar{\boldsymbol{F}} = \mathbf{1}$), note that (S4) recovers the conventional periodic boundary condition, i.e., $\boldsymbol{u}(\boldsymbol{X}+\boldsymbol{R}) = \boldsymbol{u}(\boldsymbol{R})$, where the distinction between the material and the spatial quantities disappears.

3) Implementation of Periodic Boundary Conditions in FE Framework

In order to simulate the motion of an infinitely periodic structure using a unit cell under periodic boundary condition in the FE framework, the discretized version of (S4) is constructed:[3]

$$\boldsymbol{u}_\beta = \boldsymbol{u}_\alpha + (\bar{\boldsymbol{F}} - \mathbf{1})(\boldsymbol{X}_\beta - \boldsymbol{X}_\alpha) \tag{S6}$$

where the subscripts α and β stand for two nodal points periodically located on the boundary of the unit cell. In this study, the commercial FE code ABAQUS was employed, and (S6) was implemented using the command *EQUATION. Furthermore, the components of $\bar{\boldsymbol{F}}$ can be conveniently prescribed using a set of virtual nodes and the corresponding macroscopic first Piola–Kirchhoff stress $\bar{\boldsymbol{P}}$ is then obtained through virtual work consideration.[3, 4]

Analytic Model for Capacitor with Composite Dielectric Layer

We supposed that the initial distance between two electrode is D, the initial vacuum fraction of the porous Ecoflex is f_0, the relative dielectric constant of air is $\varepsilon_{air} = 1$, and the relative dielectric constant of Ecoflex is $\varepsilon_{Ecoflex} = 2.5$.

For simplicity, we assume that the vacuum fraction f_V decreases linearly with the compressive displacement d, and becomes zero when d approaches to Df_0:[5, 6]

$$f_V(d) = \begin{cases} f_0\left(1 - \frac{d}{Df_0}\right), & if\ d \le Df_0 \\ 0, & otherwise \end{cases}. \tag{S7}$$

From a simple rule of mixture, the effective dielectric constant under compression is assumed to be:

$$\varepsilon_{effective}(d) = (1 - f_V)\,\varepsilon_{Ecoflex} + f_V\,\varepsilon_{air}\,. \tag{S8}$$

The capacitance of the parallel-plate capacitor is determined by the following equation:

$$C(d) = \varepsilon_0 \varepsilon_{effective} \frac{A}{D - d}, \tag{S9}$$

where ε_0 and A are vacuum permittivity and area of electrode, respectively.

Since ε_0, A, and D are constant during the compression, the relative change of capacitance can be calculated by the equation:

$$\frac{\Delta C}{C_0}(d) = \frac{C - C_0}{C_0} = \frac{D}{D - d} \frac{\varepsilon_{Ecoflex} + f_0\left(1 - \frac{d}{Df_0}\right)\left(\varepsilon_{air} - \varepsilon_{Ecoflex}\right)}{\varepsilon_{Ecoflex} + f_0\left(\varepsilon_{air} - \varepsilon_{Ecoflex}\right)} - 1\,. \tag{S10}$$

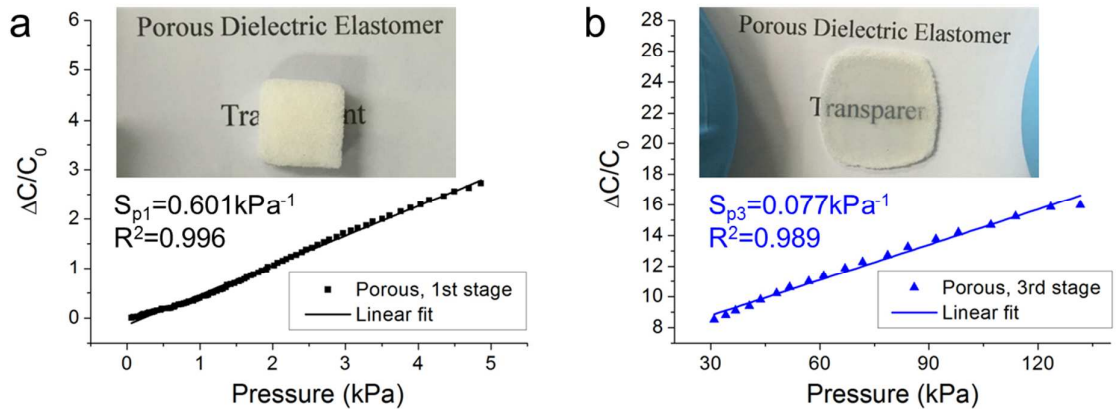

Figure S4. Linear fitting results of the first and the third stages in the pressure-response curve of the piezocapacitive pressure sensor using microporous Ecoflex dielectric layer. a) Linear fitting of the first stage showing the high sensitivity of 0.601 kPa^{-1} and R^2 = 0.996 at 0-5 kPa. The inset image shows the photograph of microporous Ecoflex with no compression, which is not transparent due to the existence of micropores. b) Linear fitting of the third stage showing lower but stable sensitivity of 0.077 kPa^{-1} and R^2 = 0.989 at 30-130 kPa. The inset image exhibits the representative photograph of microporous Ecoflex under compressive strain of ~80 %. It should be noted that the microporous Ecoflex becomes transparent like solid Ecoflex media. This implies that the internal micropores within the microporous Ecoflex cube have been closed completely like solid one.

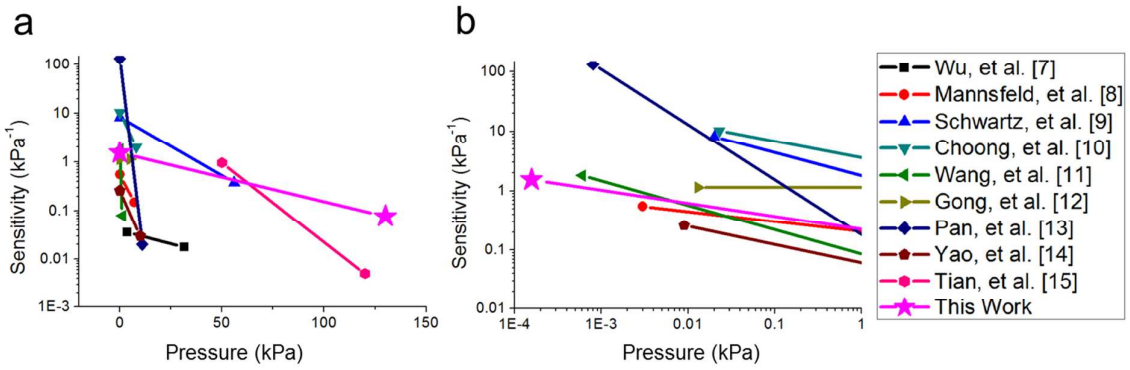

Figure S5. Comparison of the piezocapacitive pressure sensor with other state-of-the-art pressure sensors in terms of both sensitivity and detection limit a) in full-scale and b) in magnified scale near lower detection limit.[7-15]

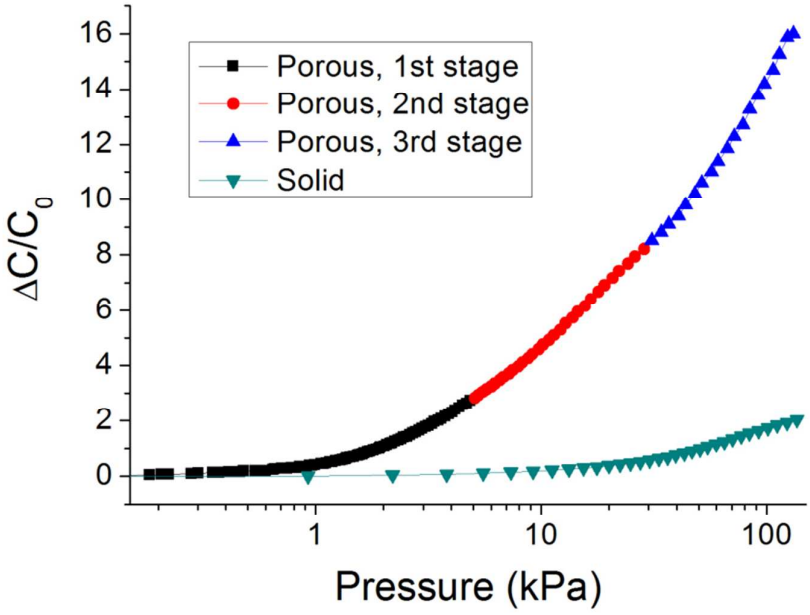

Figure S6. Log-linear plot of pressure vs. response curves (pressure in log scale and response in linear scale) of capacitive pressure sensor using solid dielectric layer and piezocapacitive pressure sensor using porous dielectric layer.

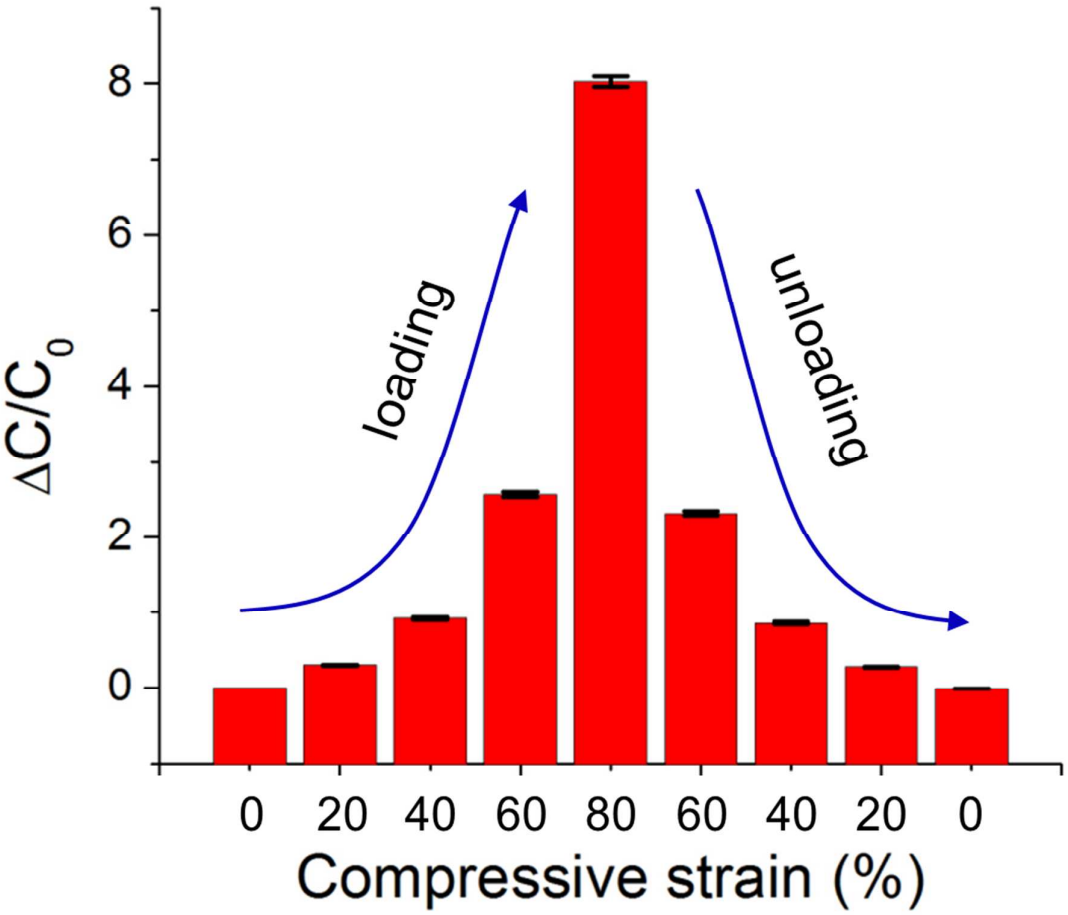

Figure S7. Reproducibility of capacitance responses of 10 different sensor samples made from each sugar cube. All sensors showed similar capacitance responses with negligible deviations from each other.

(1) Holzapfel, G. A., *Nonlinear Solid Mechanics: A Continuum Approach for Engineering*. John Wiley & Sons Ltd.: New York, 2000.

(2) Kittel, C., *Introduction to Solid State Physics*, 8th ed.; John Wiley & Sons Inc.: New York, 2005.

(3) Shim, J.; Wang, P.; Bertoldi, K. Harnessing Instability-Induced Pattern Transformation to Design Tunable Photonic Crystals. *Int. J. Solids Struct.* **2015**, *58*, 52-61.

(4) Danielsson, M.; Parks, D. M.; Boyce, M. C. Three-Dimensional Micromechanical Modeling of Voided Polymeric Materials. *J. Mech. Phys. Solids* **2002**, *50*, 351-379.

(5) Barber, P.; Balasubramanian, S.; Anguchamy, Y.; Gong, S.; Wibowo, A.; Gao, H.; Ploehn, H. J.; Zur Loye, H.-C. Polymer Composite and Nanocomposite Dielectric Materials for Pulse Power Energy Storage. *Materials* **2009**, *2*, 1697-1733.

(6) Weadon, T. L.; Evans, T. H.; Sabolsky, E. M. An Analytical Model for Porous Polymer-Ceramic Capacitive Pressure Sensors. *IEEE Sens. J.* **2014**, *14*, 4411-4422.

(7) Wu, W.; Wen, X.; Wang, Z. L. Taxel-Addressable Matrix of Vertical-Nanowire Piezotronic Transistors for Active and Adaptive Tactile Imaging. *Science* **2013,** *340*, 952-957.

(8) Mannsfeld, S. C.; Tee, B. C.; Stoltenberg, R. M.; Chen, C. V.; Barman, S.; Muir, B. V.; Sokolov, A. N.; Reese, C.; Bao, Z. Highly Sensitive Flexible Pressure Sensors with Microstructured Rubber Dielectric Layers. *Nat. Mater.* **2010,** *9*, 859-864.

(9) Schwartz, G.; Tee, B. C.; Mei, J.; Appleton, A. L.; Kim do, H.; Wang, H.; Bao, Z. Flexible Polymer Transistors with High Pressure Sensitivity for Application in Electronic Skin and Health Monitoring. *Nat. Commun.* **2013,** *4*, 1859.

(10) Choong, C. L.; Shim, M. B.; Lee, B. S.; Jeon, S.; Ko, D. S.; Kang, T. H.; Bae, J.; Lee, S. H.; Byun, K. E.; Im, J.; Jeong, Y. J.; Park, C. E.; Park, J. J.; Chung, U. I. Highly Stretchable Resistive Pressure Sensors using a Conductive Elastomeric Composite on a Micropyramid Array. *Adv. Mater.* **2014,** *26*, 3451-3458.

(11) Wang, X.; Gu, Y.; Xiong, Z.; Cui, Z.; Zhang, T. Silk-Molded Flexible, Ultrasensitive, and Highly Stable Electronic Skin for Monitoring Human Physiological Signals. *Adv. Mater.* **2014,** *26*, 1336-1342.

(12) Gong, S.; Schwalb, W.; Wang, Y.; Chen, Y.; Tang, Y.; Si, J.; Shirinzadeh, B.; Cheng, W. A Wearable and Highly Sensitive Pressure Sensor with Ultrathin Gold Nanowires. *Nat. Commun.* **2014,** *5*, 3132.

(13) Pan, L.; Chortos, A.; Yu, G.; Wang, Y.; Isaacson, S.; Allen, R.; Shi, Y.; Dauskardt, R.; Bao, Z. An Ultra-Sensitive Resistive Pressure Sensor Based on Hollow-Sphere Microstructure Induced Elasticity in Conducting Polymer Film. *Nat. Commun.* **2014,** *5*, 3002.

(14) Yao, H. B.; Ge, J.; Wang, C. F.; Wang, X.; Hu, W.; Zheng, Z. J.; Ni, Y.; Yu, S. H. A Flexible and Highly Pressure-Sensitive Graphene-Polyurethane Sponge Based on Fractured Microstructure Design. *Adv. Mater.* **2013,** *25*, 6692-6698.

(15) Tian, H.; Shu, Y.; Wang, X. F.; Mohammad, M. A.; Bie, Z.; Xie, Q. Y.; Li, C.; Mi, W. T.; Yang, Y.; Ren, T. L. A Graphene-Based Resistive Pressure Sensor with Record-High Sensitivity in a Wide Pressure Range. *Sci. Rep.* **2015,** *5*, 8603.